Materials Chemistry and Physics 257 (2021) 123712

Contents lists available at ScienceDirect

Materials Chemistry and Physics

journal homepage: www.elsevier.com/locate/matchemphys

Microwave assisted accelerated fluoride adsorption by porous nanohydroxyapatite

A.K.D. Veromee K. Wimalasiri [a], M. Shanika Fernando [a], Gareth R. Williams [b], Dhammike P. Dissanayake [a], K.M. Nalin de Silva [a], Rohini M. de Silva [a,*]

[a] Centre for Advanced Materials and Devices (CAMD), Department of Chemistry, University of Colombo, Colombo, 00300, Sri Lanka
[b] UCL School of Pharmacy, University College London, 29-39 Brunswick Square, London, WC1N 1AX, UK

HIGHLIGHTS

- Porous nano hydroxyappatite were synthesized.
- Polyvinylpyrrolidone and sodium dodecyl sulfonate template system were used.
- Fluoride adsorption onto porous hydroxyapatite is an activated process.
- Fluoride adsorption was significantly accelerated by microwave irradiation.

GRAPHICAL ABSTRACT

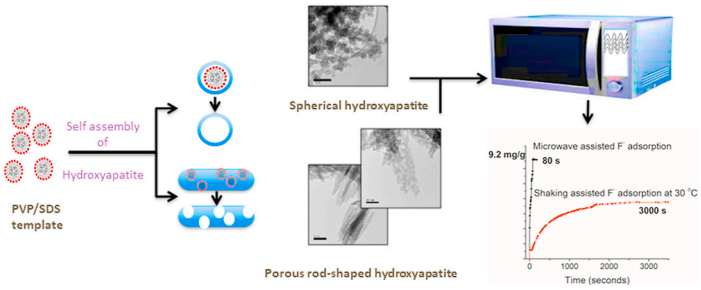

ARTICLE INFO

Keywords:
Microwave
Porous nanohydroxyapatite
Template
Fluoride
Adsorption isotherm

ABSTRACT

Fluoride pollution of water is a matter of concern in many countries due to its association with chronic kidney failure. Therefore, it is important to develop fast and efficient methods for fluoride removal from drinking water using environmentally friendly materials. In this article, the synthesis, characterization and microwave assisted accelerated fluoride removal by porous nanohydroxyapatite (PHAP) are reported. The PHAP samples were synthesized using polyvinyl pyrrolidone and sodium dodecyl sulphate micellar system as the template. The prepared nanohydroxyapatite was characterized using TEM, SEM, FT-IR, TGA, XRD and BET. Investigation of the morphology of microcrystals using TEM showed the presence of spherical particles of 20–35 nm size and highly porous rod-shaped crystals with the aspect ratio of 2:13. The adsorption of F^- ions using PHAP was carried out under the influence of microwave radiations using concentrations comparable to existing F^- levels in natural water. The equilibrium is reached within 80 s and this is the fastest saturation time recorded for any existing material. The kinetic experiments showed that the fluoride adsorption is an activated second order process. The equilibrium fluoride adsorption capacity of PHAP was found to be 9.19 mg g^{-1} at pH 6.5 for 80 s and this was proven to be a potential material to remove F^- ions rapidly from drinking water.

* Corresponding author.
E-mail address: rohini@chem.cmb.ac.lk (R.M. de Silva).

https://doi.org/10.1016/j.matchemphys.2020.123712
Received 14 July 2019; Received in revised form 15 February 2020; Accepted 16 August 2020
Available online 1 September 2020

1. Introduction

Fluoride is considered as an essential mineral with a narrow margin of safety for human wellbeing [1]. According to the WHO guidelines, the recommended fluoride concentration in drinking water is in the range of 0.5–1.5 mgL^{-1} [2]. The prolonged use of drinking water containing even a relatively low dose of fluoride have adverse effects on human health and shows dental caries even with very low concentrations such as 0.5 mg L^{-1} and greater than 10 mg L^{-1} can lead even to crippling fluorosis [3]. For example, over 90% of children in dry zone of Sri Lanka show dental fluorosis where the fluoride content in water is even less than 1 mg L^{-1} [10]. In addition, there are many reports indicating various other diseases caused by high fluoride intake such as osteoporosis [4,5], arthritis [4,6], brittle bones [4–6], infertility [4], brain damage [4], alzheimer syndrome [7] thyroid disorder, and chronic kidney disease of unknown aetiology (CKDu) [4,8]. It has also been reported that the fluoride levels over 2.0 mg L^{-1} cause increased activities of serum lactic dehydrogenase (LDH), urine N-acetyl-β-glucosaminidase (NAG), and urine γ-glutamyl transpeptidase (γ-GT) in children and damage liver and kidney functions [9].

Thus, the ingestion of elevated fluoride concentrations via drinking water is a matter of concern. Both natural and anthropogenic activities contribute to increase the fluoride content in drinking water. Many fluoride containing minerals and rocks such as fluorite, topaz, biotite, cryolite, granite, shale, basalt and syenite are widely distributed in the earth's crust [11]. Although these rocks and minerals are hardly soluble in water at neutral pH, when the conditions are changed, fluorides can be leached to the ground water [10,11]. In addition, various industrial effluents containing high fluoride concentrations and also contribute to increased levels of fluoride in water [12].

Therefore, the removal of excess fluoride from drinking water systems has received much attention and various treatment techniques such as chemical precipitation [13], adsorption [14,15], reverse osmosis [16–18], nanofiltration [19], and electrodialysis [20,21] have been employed for water defluorination. Among these methods, adsorption is a promising technology due to its simplicity of design, operation and cost effectiveness. Activated alumina [22,23], calcium based materials [24–26], iron-based sorbent materials [27,28], metal oxides/hydroxides/oxyhydroxides/metal-impregnated oxides [29,30], carbon based materials [29,31], layered double hydroxides [32–34], and hydroxyapatite [35,36], have been considered as attractive sorbents in defluorination. Among the variety of materials used for defluorination, hydroxyapatite (HAP) has been identified as one of the promising materials for the removal of fluoride from water mainly due to cost-effectiveness and biocompatibility. Moreover, the application of variety of morphologically different HAP in water defluorination, such as nano HAP [37–39], porous HAP [40,41]' nanowires [42]' nanorods of HAP [38,43] and also hollow nano HAP [44,45] has been reported. The facile synthesis of hydroxyapatite with complex and fascinating morphologies requires mimicking of the natural biomineralization process [46]. Therefore, the organic templates with complex functional patterns were used to control the nucleation, growth and alignment of inorganic crystals [47,48].

The objective of our study was to investigate the effect of microwave energy on fluoride adsorption onto porous nano HAP as it has never been considered for HAP systems. In addition, the possibility of removing F^- ions at concentrations existing in natural water at natural pH conditions were investigated as almost all the existing literature work has dealt with very high concentrations of F^- using low pH conditions. For this purpose, the hollow microspheres/nanospheres of hydroxyapatite and highly porous nanorod assembled crystals of hydroxyapatite were synthesized using polyvinyl pyrrolidone and sodium dodecyl sulphate (PVP/SDS) template assisted system. The synthesized material was tested for fluoride removal from aqueous solutions and was found that the adsorption process can be significantly enhanced by increasing the kinetic energy using microwave.

2. Experimental

2.1. Materials

All the chemicals used in this study were of analytical grade and they were used without any further purification. Polyvinylpyrrolidone (PVP) average molecular weight 10,000 and sodium dodecyl sulfonate (SDS, 98%) were purchased from Sigma-Aldrich Ltd. Calcium nitrate tetrahydrate (98%) from Techno Pharmchem, India was used in the synthesis along with ammonium monohydrogen phosphate (99%, Sigma Aldrich). Sodium fluoride (99.5% Merck) was used to prepare fluoride stock solution.

2.2. Synthesis of porous nanohydroxyapatite (PHAP)

Porous nanohydroxyapatite was synthesized by the wet chemical precipitation method. Briefly, the template for the synthesis was prepared by adding 25 ml of 20 g/L PVP and 25 ml of 60 mM SDS into a three neck flask. The mixture was heated up to 60 °C and stirred for 1 h. To this solution, 0.4 M $Ca(NO_3)_2.4H_2O$ and 0.15 M $(NH_4)_2HPO_4$ in 1.67 Ca/P molar ratio were added dropwise while stirring. During the process, pH of the medium was maintained at 10 using 3.5 M NH_4OH solution. The reaction mixture was maintained at 80 °C for 3 h under vigorous stirring. The mixture was aged for 24 h, then it was centrifuged and washed several times using distilled water and dried.

2.3. Characterization of the samples

The morphological and structural studies of synthesized PHAP samples were conducted using Scanning Electron Microscopy (HITACHI SU6600, at 15.0 kV). The transmission electron microscopic analysis (TEM) was carried out using JEOL JEM 2100 electron microscope. The presence of functional groups of nanohydroxyapatite was confirmed by studying the sample using a FT-IR spectrometer (Varian 660-IR) in the wavenumber range of 500–4000 cm^{-1}. The X-ray powder diffraction patterns of the samples were obtained using a Bruker D8 Focus X-Ray-Diffractometer using Cu Kα radiation (0.154 nm) over the 2Θ range of 2°–80°, with a step size of 0.02°. The thermal gravimetric analysis for the respective samples was carried out using a thermogravimetric analyzer (TGA SDT Q 400) in the temperature range from room temperature to 600 °C. The surface area of synthesized PHAP was measured by BECKMAN COULTER SA3100 BET analyzer.

2.4. Adsorption study

The stock solution of fluoride was prepared by dissolving 5.0 g of sodium fluoride in 1 L distilled water in a PVC container. The experimental solutions for adsorption and analysis were freshly prepared by diluting F^- stock solution with distilled water. All the experiments were conducted using vessels made of polypropylene or PVC. The total ionic strength adjusting buffer (TISAB-III) solution was added to all the samples (1:1) before measuring the fluoride concentrations using a fluoride selective electrode (Orion ion selective electrode).

2.4.1. Influence of pH on the fluoride uptake capacity

The influence of the pH on fluoride uptake capacity was investigated by controlling the pH level of the system from 1 to 13 using 0.1 M HCl and 0.1 M NaOH. The solution pH and concentration of fluoride were determined using a pH electrode and a fluoride ion selective electrode, respectively.

2.4.2. Adsorption kinetic study

The adsorption kinetic studies were carried out using two different methods (Method 1 and Method 2).

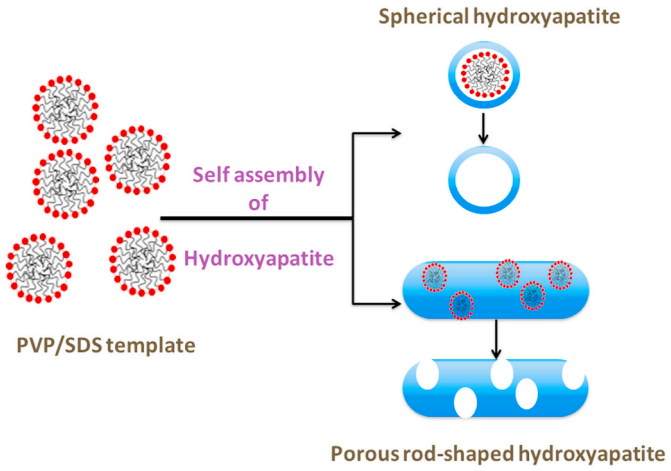

Fig. 1. Self - assembly of hydroxyapatite.

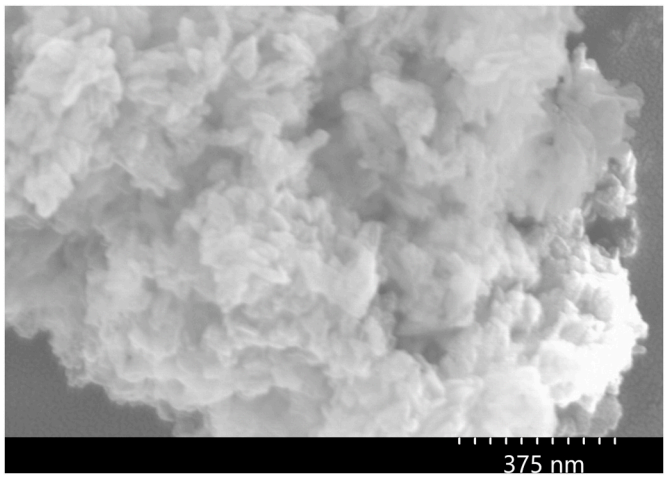

Fig. 2. SEM image of porous hydroxyapatite (PHAP).

2.4.2.1. Method 1. Adsorption of fluoride by porous nano-hydroxyapatite was continuously monitored using fluoride ion selective electrode at three different temperatures. Adsorption of fluoride by 0.04 g of porous nanohydroxyapatite from a 5 ppm solution (20 ml) was studied at 30, 50 and 80 °C for 2 h with continuous stirring at 180 rpm.

2.4.2.2Method 2.

Polypropylene vials containing 20 ml of 5 ppm fluoride solution and 0.04 g of porous nanohydroxyapatite was exposed to microwave radiation (180 W of SAMSUNG TDS microwave, 230 V) for a predetermined time (from 5 to 120 s). The residual fluoride levels were measured using the fluoride ion selective electrode.

2.4.3. Adsorption isotherms

In the adsorption isothermal studies, 0.02 g of porous nano-hydroxyapatite was added to 10 ml of fluoride solution at the concentrations ranging from 1 to 20 ppm (1, 3, 5, 10, 15 and 20 ppm) and the solution pH was adjusted to 6.8. After exposing it to microwave energy for 80 s, the residual fluoride concentration was measured using the fluoride ion selective electrode. In addition, the adsorption studies were carried out with higher concentrations of F^- (150 and 200 ppm) (Fig. S2) in order to compare adsorption capacities obtained at higher concentrations in reported works.

3. Results and discussion

3.1. Characterization of PHAP

In the aqueous system, SDS molecules start to form micelles at critical micelle concentration (CMC) by arranging their head groups toward the surrounding medium while directing the hydrophobic tail regions in the micelle center. CMC of SDS surfactant is 8.3 mM at 25 °C and it increases with increasing temperature [49,50]. In this study, 60 mM concentration of SDS was used and the reaction medium was heated up to 60 °C. It is reported that the CMC value of SDS at 60 °C is 9.2 mM [49,51]. The used concentration of SDS is 60 mM and it is about 6 times greater than the CMC value of SDS at 60 °C. It is very important to maintain the system with high SDS concentration in order to obtain higher amounts of micelles [52]to increase the porous nature of HAP. As described earlier, during the nucleation process, these micelles act as templates as well as nucleation sites for HAP crystallization. Higher the number of micelles trapped inside HAP, higher would be the porosity of HAP.

The driving force for the micelle formation is the minimization of contact between water and hydrophobic tail region. The thermodynamic feasibility of the micelle formation can be expressed as follows [49],

$$\Delta G^{\circ} = -RTln(CMC) \quad (1)$$

The free energy change for the micelle formation at 60 °C is approximately −13 kJ mol^{-1}.

PVP molecules can strongly interact with anionic SDS head group to form PVP-SDS spherical shaped complex micelles [53,54] (Fig. 1). Furthermore, the calcium ions in the medium also have very high affinity towards these anionic head groups and, therefore, these SDS molecules in the PVP-SDS complex micelles provide nucleation sites for the crystallization of hydroxyapatite.

The scanning electron micrograph (SEM) of nanohydroxyapatite synthesized in the presence of the polymer-surfactant template (PVP/SDS) is shown in Fig. 2. According to the image, there are rod shaped and spherical shaped particles and they are combined or agglomerated in such a way to provide many pores/groves to give a complex hollow nature. In addition, the sample surface is uneven providing a high surface area with nanogrooves of the size ranging over 80–200 nm. This is in contrast with the morphology of rod shaped hydroxyapatite nanoparticles synthesized using the same conditions in the absence of the PVP/SDS template [38]. Therefore, it is very clear about the template effect of PVP/SDS to provide hollow morphology of nanohydroxyapatite.

The porous nature of synthesized HAP was further confirmed using transmission electron microscopy (TEM), as shown in Fig. 3. The formation of both spherical and rod shape nanoparticles can be observed in these micrographs (Fig. 3 (a) and (b)). A careful observation of Fig. 3(c) shows the existence of a spongy nature having tiny holes connected and spread along each particle giving a porous structure. Moreover, the size range of the spherical shaped hydroxyapatite is approximately 20–35 nm in diameter and the aspect ratio of rod shaped nanoparticles is 2:13.

The FTIR spectra of unwashed and washed PHAP samples are shown in Fig. 4. The IR adsorption bands at 3464 cm^{-1} and 1652 cm^{-1} can be attributed to the bending vibration mode of H bonded OH groups present in hydroxyapatite. The peak at 1020 cm^{-1} corresponds to the stretching mode of PO_4^{3-} groups and the peaks at 601 and 850 cm^{-1} are the bending modes of PO_4^{3-} groups [38,55,56]. The assignment of vibrational frequencies observed in the IR spectra is given in Table S1. The IR band appeared in the region of 1350-900 cm^{-1} is a combination of several overlapping peaks such as CH_2 wagging, SO_2 asymmetric stretching and the vibrational modes associated with phosphate groups and CN bond vibrations of PVP. The FT-IR spectrum of the washed PHAP does not show the IR absorptions related to PVP/SDS. The absence of IR bands correspondent to both PVP and SDS in washed PHAP (Fig. 4) confirmed their absence on the surface. However, the template of PVP/SDS present deep inside the PHAP particle may have not being removed during the washing process as indicted in the TGA analysis

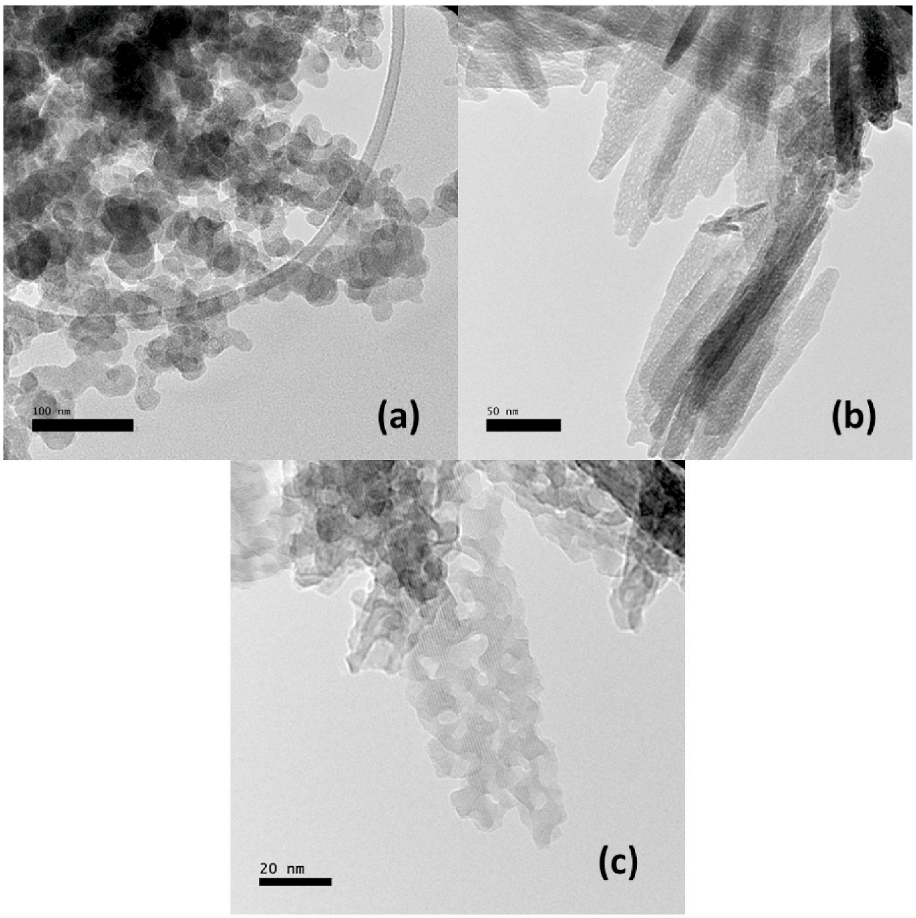

Fig. 3. TEM images of porous microspheres/rods of hydroxyapatite. (a) Spherical shaped hydroxyapatite, (b) and (c) Porous rod-shaped hydroxyapatite at different magnifications.

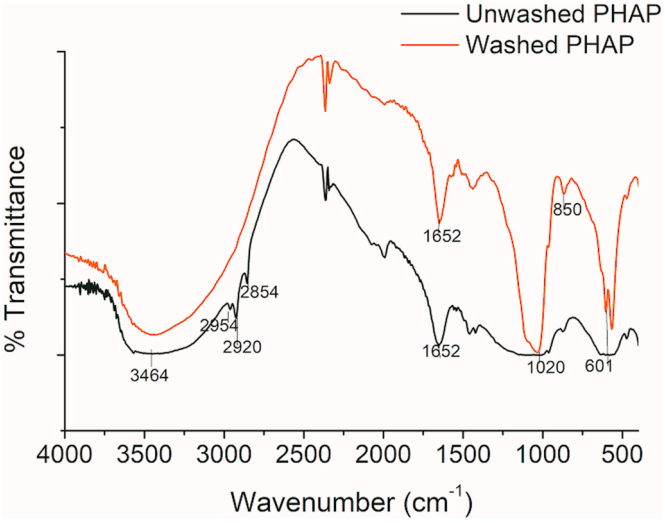

Fig. 4. FT-IR spectra of (a) washed PHAP and (b) unwashed PHAP.

given in Fig. 5.

In this study, TGA was accomplished under nitrogen and oxygen environments separately. Weight loss corresponding to PVP and SDS [57–59] were identified as 2.54% at the temperature range of 220–400 °C and 3% at the temperature range of 215–540 °C for nitrogen and oxygen environments respectively.

Further, the specific surface area of PHAP was measured by Beckman Coulter Sorption Analysis and it was found that surface area of PHAP is 41.3 m^2/g. The X ray powder diffraction pattern of porous nano-hydroxyapatite is given in Fig. 6 and it contains peaks at 2Θ positions of 26, 31, 32, 34, 39 and 50° and the results are in good agreement with hydroxyapatite [56,60].

3.2. The influence of microwave energy and temperature on the adsorption process of fluoride onto PHAP

Adsorption of fluoride by nanohydroxyapatite at neutral pH is shown in Fig. 7. It can be observed that the rate of F^- adsorption increases with increasing temperature and levels off around 1.2 mg g^{-1} at 5 ppm initial fluoride concentration. It can also be observed that the system takes a long time to reach equilibrium at room temperature. The strong dependence of fluoride adsorption on temperature indicates that it is an activated process. Therefore, an attempt was made to accelerate the process by providing microwave irradiation. The system was exposed to microwave radiation (180 W) for 80 s and the adsorption of fluoride was monitored.

The effect of different methods used to accelerate the fluoride adsorption is shown in Fig. 8. It can be observed that the exposure to microwave energy dramatically increases the rate of fluoride adsorption. It was also worth noticing that, with normal stirring mode at 5 ppm initial fluoride level, the system required more than 5 min at 80 °C to reach its equilibrium capacity of 1.2 mg g^{-1} (Fig. 8), whereas, with microwave energy, it took only 1 min to reach the capacity of 1.35 mg g^{-1}. We can suggest two reasons for the increased adsorption of F^- under the microwave treatment. When the fluoride-nanohydroxyapatite

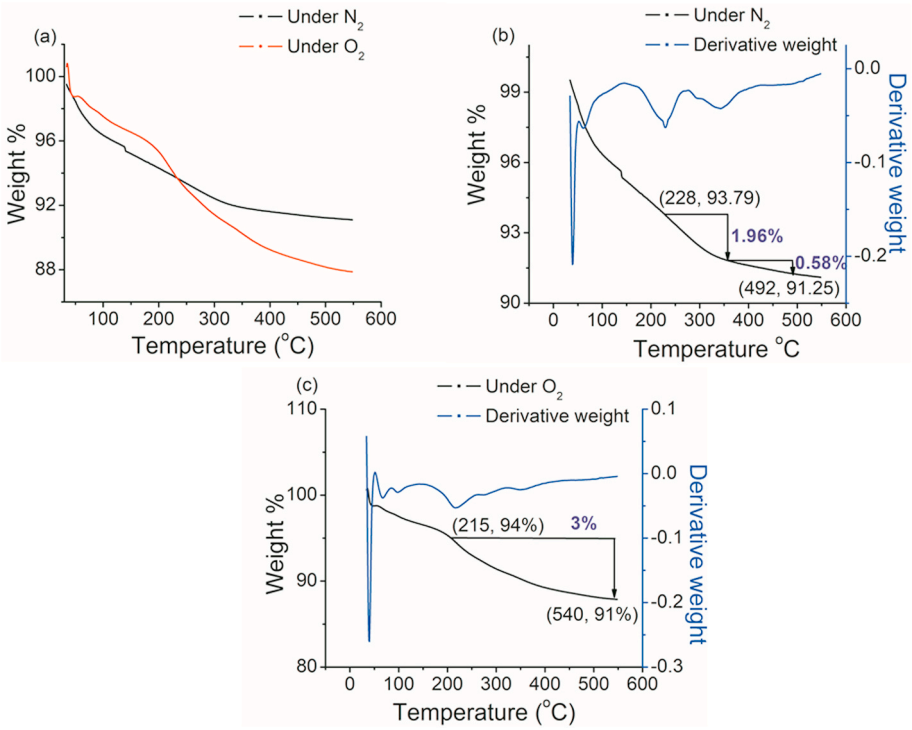

Fig. 5. Thermogravimetric curves for the decomposition of washed PHAP (a) Percentage weight loss as a function of temperature, (b), (c) Derivatives of the weight loss temperature curves.

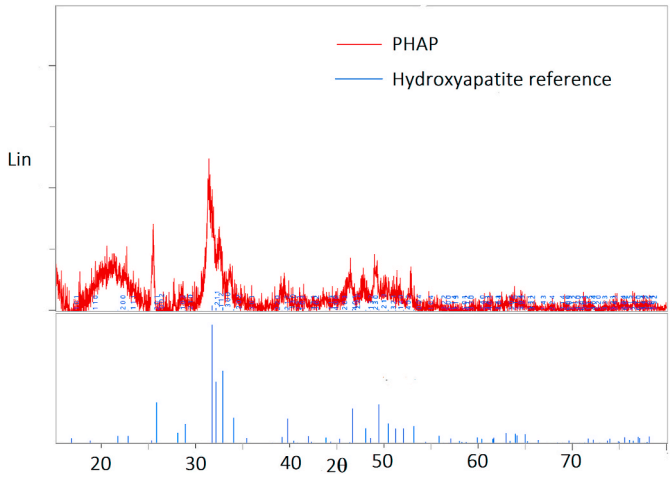

Fig. 6. XRD spectrum of PHAP.

aqueous system is subjected to microwave irradiation, the molecular dipole rotations occur. These rotating water molecules can push, pull or collide with other molecules and thereby distribute the dielectric heating energy to adjacent fluoride ions to overcome the activation energy barrier. In addition, the increased oscillations and collisions of water molecules in the hydration sphere of fluoride may temporarily expose F^- ions to HAP surface to promote the adsorption.

3.3. Influence of pH on the fluoride uptake capacity

The influence of pH on the fluoride removal by nanohydroxyapatite was investigated in the pH range of 1–13. As shown in Fig. 9, the equilibrium sorption capacity increased with increasing pH and reached a maximum at pH = 6.5 which is equal to pH of drinking water. Less fluoride adsorption at low pH can be attributed to the dissolution of

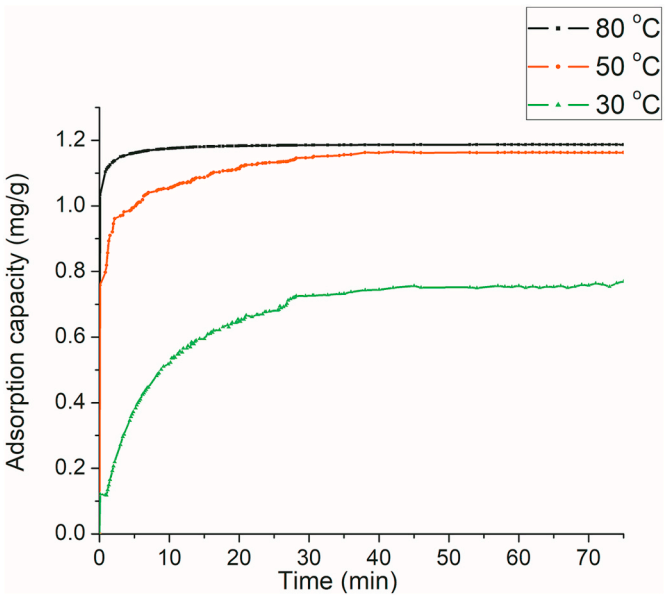

Fig. 7. The amount of fluoride adsorbed vs. time at 5 ppm initial fluoride concentration at (a) 80 °C, (b) 50 °C and (c) 30 °C.

apatite as shown in equation (2), resulting unstable sorbent surface as well as having increased competition for F^- ions due to the releasing of HPO_4^{2-}.

$$Ca_{10}10(PO_4)_6(OH)_2 + 8H^+ \rightleftharpoons 10Ca^{2+} + 6HPO_4^{2+} + 2H_2O \quad (2)$$

At extremely high pH, competition of hydroxide ions causes a slight decrease in fluoride adsorption.

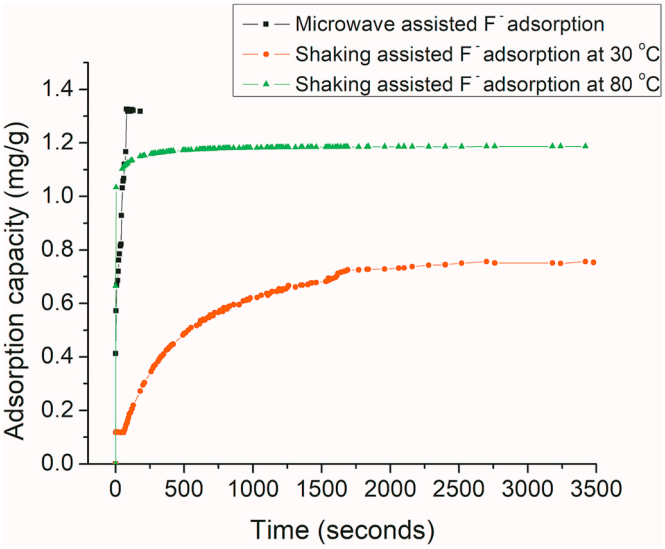

Fig. 8. The effect of different methods on the equilibrium time and adsorption capacity of PHAP.

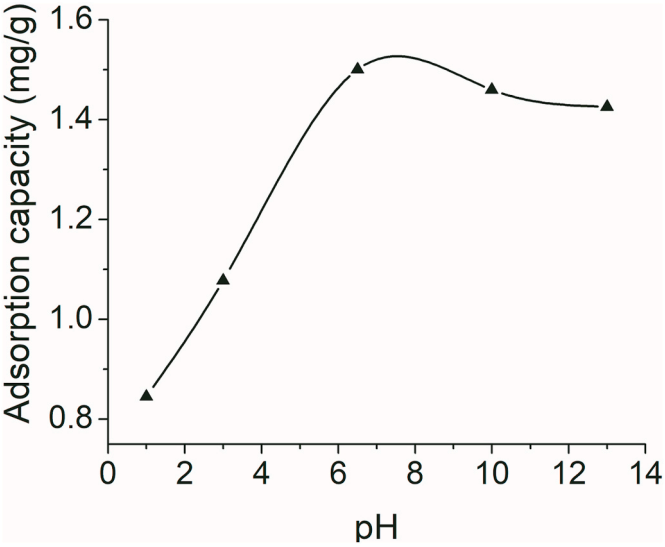

Fig. 9. Effect of solution pH on fluoride adsorption at 5 ppm initial fluoride level.

3.4. Adsorption dynamics and mechanism

As shown in Figs. 2 and 3, the surface of porous nanohydroxyapatite synthesized in the presence of PVP/SDS template system is coarse. The adsorption of solute from solution by porous adsorbents is a multi-step process which involves a bulk transport of solute, film transport of solute and diffusion through a hypothetical film boundary layer and finally the diffusion of solute within pores and along pore wall surfaces to an active adsorption sites [61].

Therefore, when fluoride-hydroxyapatite system is subjected to microwave irradiation, the energy transfer via collisions could accelerate the diffusion/adsorption processes. To our knowledge, the enhancement of fluoride adsorption by microwave radiation has not been reported previously. Efficacy of sorption depends on sorption capacity and sorption rate. These are useful parameters and can be determined from a kinetic analysis of the system. These kinetic data are useful in designing fast and effective sorption systems for fluoride removal. The fluoride-porous nanohydroxyapatite system was studied using four kinetic

Table 1
Parameters of Lagergren-first-order and Pseudo second order for fluoride adsorption from 5 ppm initial fluoride solution.

Kinetic models	Parameters	Temperature		
		80 °C	50 °C	30 °C
Lagergren-first-order	q_e (mg g^{-1})	0.05	0.31	0.67
	k_1 (min^{-1})	0.12	0.09	0.06
	R^2	0.9176	0.9433	0.9657
Pseudo second order (t/q_t vs. t)	q_e (mg g^{-1})	1.19	1.13	0.79
	k_2 (min^{-1})	8.86	1.62	0.27
	R^2	0.9999	0.9992	0.9796
Experimental adsorption capacity (q_e) for 5 ppm fluoride solution	q_e (mg g^{-1})	1.26		

Table 2
Parameters of Intra particle diffusion and Boyd's model for fluoride adsorption by PHAP from 5 ppm initial fluoride solution.

Boyd's model				
Temperature (°C)	B (min^{-1})	$D_{eff.}$ (cm^2 min^{-1})* 10^{-13}	R^2	Intercept/thickness of boundary layer
30	0.02	1.2	0.99	−0.03
50	0.091	2.3	0.92	0.91
80	0.15	3.7	0.96	2.52
Intra particle diffusion model				
Temperature (°C)	k_{in} (mg/ $gmin^{-1/2}$)	D (cm^2 min^{-1}) *10^{-14}	R^2	Intercept/thickness of boundary layer
30	0.15	2.45	0.97	0.02
50	0.07	0.35	0.90	0.84
80	0.02	0.022	0.74	1.10

models namely, Lagergren-first-order model, Ho's pseudo-second-order model, Weber's and Morris's intra-particle diffusion model and Boyd's model [62,63].

The integrated form of Lagergren-first-order rate expression can be presented as follows:

$$\ln(q_e - q_t) = \ln q_e - k_1 t \tag{3}$$

Where q_e and q_t are the amounts of fluoride adsorbed (mg/g) at equilibrium and at time t, respectively and k_1 is the rate constant of the adsorption process.

The integrated form of the pseudo second order kinetic model is as follows:

$$\frac{t}{q_t} = \frac{1}{k_2 q_e^2} + \frac{t}{q_e} \tag{4}$$

Where q_e and q_t are the amounts of fluoride adsorbed (mg/g) at equilibrium and at time t, respectively and k_2 is the rate constant of pseudo second order adsorption process [53–55]. The kinetics of fluoride adsorption was tested by fitting data to the models described above and the results are reported in Tables 1 and 2. It can be seen that the adsorption of fluoride onto PHAP agrees well with pseudo second order kinetic model [64–66].

The kinetic data were also fitted to the Boyd's film diffusion model and intra particle diffusion model of Morris and Weber in order to obtain an insight into the mechanism and rate determining steps of fluoride adsorption.

The Boyd film diffusion model can be used to investigate whether the main resistance to mass transfer is the diffusion through the boundary layer surrounding the adsorbent particle, or the resistance to diffusion inside the pores [67–69]. This model is given by the equation:

$$F = 1 - \frac{6}{\pi^2} \sum_{n=1}^{\infty} \frac{1}{n^2} \exp(-n^2 B_t) \tag{5}$$

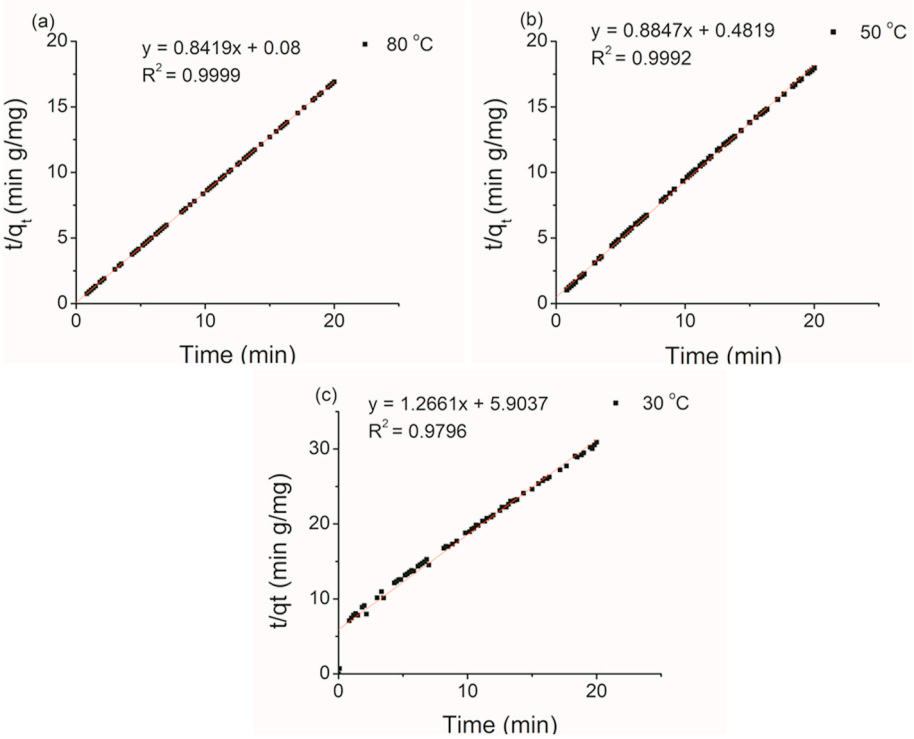

Fig. 10. Pseudo second order kinetic model at three different temperatures, (a) at 80 °C (b) at 50 °C (c) at 30 °C.

Where, B_t is the rate coefficient and F is fractional attainment of equilibrium at time t. In this model, B_t is taken to be a function of F.

$$F = \frac{q_t}{q_e} \tag{6}$$

Where q_e and q_t are the amounts of fluoride adsorbed (mg/g) at equilibrium and at time t, respectively. The Fourier transformation of Boyd equation generates the following two relations:

$$B_t = \left(\sqrt{\pi} - \sqrt{\pi - \left(\frac{\pi^2 F}{3}\right)}\right)^2 \text{ For F } < 0.85 \tag{7}$$

$$B_t = -0.4977 - \ln(1 - F) \text{ or } F > 0.85 \tag{8}$$

Where the rate coefficient B_t is related to the effective diffusion coefficient (D_e) and the particle radius (r) as given in the following equation:

$$B_t = \frac{\pi^2 D_e}{r^2} \tag{9}$$

Where, the shape of the particle has been assumed as spherical.

A plot between time and B_t is used to explain the adsorption mechanism. If the plot is linear and passes through the origin, the rate of mass transfer is assumed to be controlled by the pore diffusion. If the plot is nonlinear or linear but does not pass through the origin, the adsorption process is assumed to be controlled by a chemical reaction or film diffusion process.

Intraparticle diffusion model investigates whether the intraparticle diffusion of solute is the rate determining step. In this case, the rate is partially a function of the pore size distribution of the adsorbent and the structure of the solute. The intraparticle diffusion model is described by the equation below:

$$q_t = k_{in} t^{0.5} \tag{10}$$

Where q_t (mg/g) is the adsorption capacity at time t, k_{in} (mg/g $min^{-0.5}$) is the intraparticle diffusion rate constant and $t^{0.5}$ is the square root of time [70].

The intra particle diffusion coefficient (D) can be calculated from the following equation [71],

$$k_{in} = \frac{6q_e}{R}\sqrt{\frac{D}{\pi}} \tag{11}$$

Where R (cm) is the particle radius, q_e (mg/g) is the adsorption capacity at equilibrium. D was calculated by assuming all the particles are spherical in shape. In this case, the slope of q_t versus $t^{0.5}$ graph gives k_{in} and the average particle radius was determined by analyzing TEM images.

In order to predict the mechanism of fluoride adsorption onto PHAP, the kinetic data were analysed by the kinetic models described above. The values of kinetic parameters and correlation coefficients obtained with the models are listed in Tables 1 and 2 The best correlation was obtained with the pseudo second order model for the adsorption of fluoride onto nanohydroxyapatite. The graphs in Fig. 10 show the agreement of experimental data with the second order kinetic model at three different temperatures.

It has been reported that there are three possible mechanisms to explain the uptake of free fluorides by nanohydroxyapatite. They are the substitution into the crystal lattice, adsorption on the surface, and precipitation. The mechanism of fluoride uptake and efficiency of fluoride removal are strongly dependent on the morphology of PHAP and chemical composition of water (pH, concentration of ions in solution) [72,73]. As the ionic radii of fluoride (1.36 Å) and hydroxyl (1.40 Å) are comparable, the substitution of hydroxyl by fluoride in the hydroxyapatite lattice is not sterically hindered. The centre of the calcium triangles in the hydroxyapatite lattice can comfortably accommodate the fluoride ion due to its small size. Furthermore, the substitution of fluoride at the centre of calcium triangle eliminates the electric dipole present in the lattice due to off centred position occupied by hydroxyl ion yielding a thermodynamically more stable lattice structure. Although, the surface charge plays an important role on the adsorption of fluoride, it has been reported that the fluoride adsorption by nanohydroxyapatite is mainly controlled by the diffusion of fluoride into the hydroxyapatite crystal

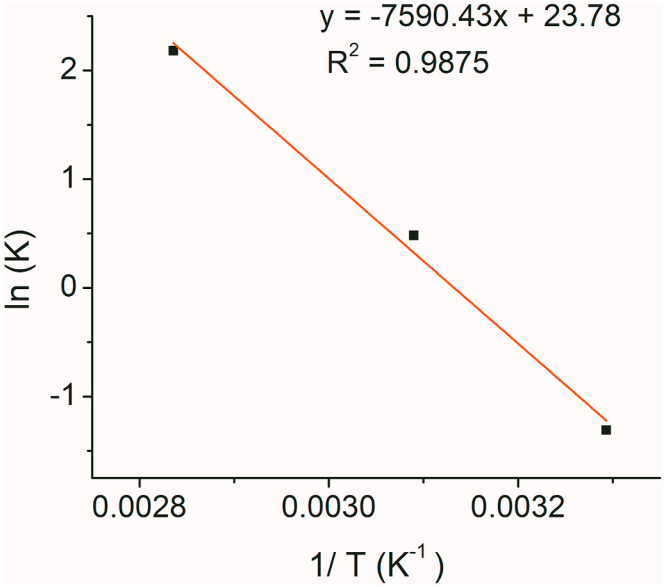

Fig. 11. Arrhenius plot for fluoride adsorption onto PHAP.

[72,73].

3.5. Temperature dependence and activation energy

The fluoride adsorption rate increases with increasing temperature, indicating that this process is an activated process. Therefore, the Arrhenius equation was used to estimate the apparent activation energy of adsorption process [74].

$$k = Ae^{\frac{-E_a}{RT}} \tag{12}$$

Where k is the rate constant, A is the Frequency factor, E_a is the activation energy, T is the temperature in kelvin and R is the universal gas constant.

The apparent activation energy calculated using Arrhenius equation for the fluoride adsorption by nanohydroxyapatite (Fig. 11) is equal to 63.1 kJmol^{-1}.

3.6. Adsorption isotherms

The adsorption isotherm models such as Langmuir and Freundlich can be used to describe the adsorption process at equilibrium [62]. The Langmuir isotherm equation describes the formation of a saturated monolayer of adsorbate on the surface of the adsorbent at the equilibrium. In order to apply this model, the surface of the adsorbate should have energetically equivalent and identical binding sites.

Table 3
Isotherm parameters of PHAP.

Experimental data at 20 ppm initial fluoride concentration	q_e (mg/g)	12.29
Langmuir model	q_e (mg/g)	16.69
	K_1 (min^{-1})	0.17
	R^2	0.41
Freundlich model	q_e (mg/g)	9.19
	K_f (g mg^{-1} min^{-1})	2.33
	R^2	0.96
	n	1.54

The simplified form of the Langmuir isotherm equation can be expressed as,

$$\frac{C_e}{q_e} = \frac{C_e}{q_m} + \frac{1}{Kq_m} \tag{13}$$

Where C_e (mg/L) is equilibrium fluoride concentration, q_e is the equilibrium amount of fluoride adsorbed, q_m is the maximum adsorption capacity of the adsorbent and K (L mg^{-1}) is the equilibrium constant of the adsorption process.

The Freundlich adsorption isotherm explains the adsorption process at equilibrium on a heterogeneous surface. The Freundlich isotherm equation in linear form can be expressed as,

$$\ln q_e = \ln K_f + \frac{1}{n}\ln C_e \tag{14}$$

Where C_e (mg/L) is equilibrium fluoride concentration, q_e is amount of fluoride adsorbed at the equilibrium K_f (L/mg) is the empirical constant of Freundlich isotherm which depends on temperature and n is the empirical parameter related to the intensity of adsorption. Values of "n" between 1 and 10 can be considered as a favourable conditions for adsorption [75].

The experimental data fitted to Langmuir and Freundlich isotherm models are shown in Fig. 12 and a better agreement of experimental data to Freundlich model is revealed. The parameters of isotherms are given in Table 3. These results show that the adsorption occurs on a heterogeneous surface and the binding sites of PHAP for fluoride ions are not energetically equivalent. Accordingly, the adsorption capacity was found to be 9.19 mg g^{-1}. In addition, the reported material was engineered in such a way that it could efficiently adsorb fluoride at the pH of drinking water. It is also worth mentioning that this material showed high adsorption capacities (54 mg g^{-1}) at high fluoride concentrations (200 ppm) and also it can reached the equilibrium within 80 s at drinking water pH (Supporting document S2). In contrast to our investigation, many of the synthesized adsorbents to remove F^- in reported data, to date show their highest capacities at very low pH diminishing

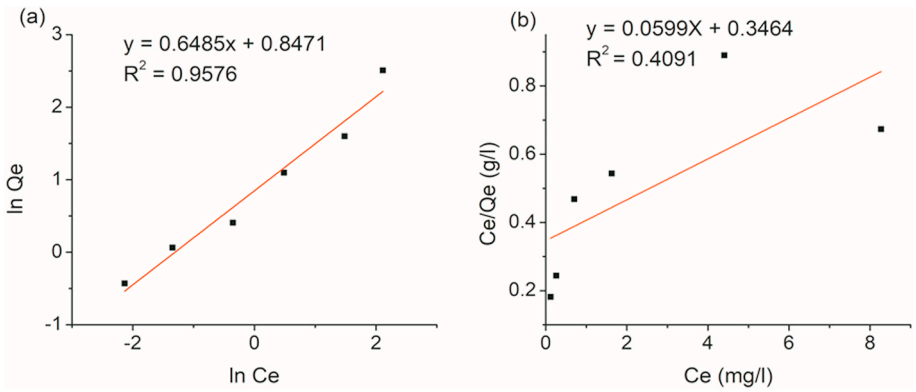

Fig. 12. Sorption isotherms for Fluoride adsorption onto PHAP (a) Freundlich isothermal model (b) Langmuir model.

Table 4
The adsorption conditions reported for already published materials.

Material	Shaking time	pH	Initial concentration which was used for adsorption isotherms (mg/L)	Maximum adsorption capacity (mg/g)	Adsorption isotherm model	Reference
GC ($FeSO_4{\cdot}7H_2O$)	48 h	6.9	5–50	2.16	Langmuir model	[62]
GC (Fe_2O_3)	48 h	6.9	5–50	1.7		
CeO_2–ZrO_2 nanocages	24 h	4	1–100	175	Langmuir model	[76]
CeO_2/Mg–Fe layered double hydroxides	24 h	6–7	20–200	60.4	Langmuir model	[32]
Mineral- substituted hydroxyapatite	60 min	3	10	8.36	Langmuir model	[77]
Porous nanohydroxyapatite	**80 s**	6.8	1–20	9.19	Freundlich model	(This work)
	80 s	6.8	200	54		

their applicability in real drinking water applications

The adsorption capacities, initial concentrations, pH and time taken to reach the equilibrium for reported materials are summarized in Table 4. According to these data, our material reached equilibrium within 80 s under the influence of microwave and this value is the fastest ever recorded for fluoride adsorption.

4. Conclusion

The porous hydroxyapatite (PHAP) was successfully synthesized using PVP-SDS template system. The fluoride adsorption on porous nanohydroxyapatite was an activated process which followed second order kinetics and could be accelerated using microwave energy. The time taken to reach the equilibrium (more than 15 min at 30 °C) could be reduced to 80 s by exposing to microwave irradiation providing the fastest F^- adsorption system for ever recorded. As PHAP shows its highest capacity at pH 6–7, this system has a very high potential in defluorination of drinking water.

CRediT authorship contribution statement

A.K.D. Veromee K. Wimalasiri: Writing - original draft, Writing - review & editing, Supervision, conceived the idea, designed the experiments, carried out the experiments and wrote the first draft of the paper, are PhD students and supervised by, All authors discussed the results and commented on the final manuscript and agreed to publish in Materials Chemistry and Physics. **M. Shanika Fernando:** Formal analysis, Data curation, Supervision, designed the experiments, contributed towards characterization of materials and analysis of data, PhD students and supervised by. **Gareth R. Williams:** Formal analysis, Data curation, contributed towards characterization of materials and analysis of data. **Dhammike P. Dissanayake:** Formal analysis, Data curation, contributed towards characterization of materials and analysis of data. **K.M. Nalin de Silva:** Writing - review & editing, Supervision, designed the experiments, supervised the project and edited the final draft of the manuscript, PhD students and supervised by. **Rohini M. de Silva:** Writing - review & editing, Supervision, conceived the idea, designed the experiments, supervised the project and edited the final draft of the manuscript.

Declaration of competing interest

The authors declare that they have no known competing financial interests or personal relationships that could have appeared to influence the work reported in this paper.

Acknowledgements

The authors gratefully acknowledge the National Research Council Sri Lanka (NRC TO 16–18) for the financial support provided and the Sri Lanka Institute of Nanotechnology for conducting the Transmission Electron microscope (TEM) and Scanning electron microscope (SEM) studies.

Appendix A. Supplementary data

Supplementary data to this article can be found online at https://doi.org/10.1016/j.matchemphys.2020.123712.

References

[1] M. Mohapatra, S. Anand, B.K. Mishra, D.E. Giles, P. Singh, Review of fluoride removal from drinking water, J. Environ. Manag. 91 (2009) 67–77, https://doi.org/10.1016/j.jenvman.2009.08.015.
[2] H. Liu, S. Deng, Z. Li, G. Yu, J. Huang, Preparation of Al-Ce hybrid adsorbent and its application for defluoridation of drinking water, J. Hazard Mater. 179 (2010) 424–430, https://doi.org/10.1016/j.jhazmat.2010.03.021.
[3] S. Dey, S. Goswami, U.C. Ghosh, Hydrous Ferric Oxide (HFO) - A Scavenger for Fluoride from Contaminated Water, 2004, https://doi.org/10.1023/B:WATE.0000044854.71497.b6.
[4] V. Dhar, M. Bhatnagar, Physiology and toxicity of fluoride, Indian J. Dent. Res. 20 (2009) 350, https://doi.org/10.4103/0970-9290.57379.
[5] J. Aaseth, M. Shimshi, J.L. Gabrilove, G.S. Birketvedt, Fluoride: a toxic or therapeutic agent in the treatment of osteoporosis? J. Trace Elem. Exp. Med. 17 (2004) 83–92, https://doi.org/10.1002/jtra.10051.
[6] D. Chakraborti, M.M. Rahman, A. Chatterjee, D. Das, B. Das, B. Nayak, A. Pal, U. K. Chowdhury, S. Ahmed, B.K. Biswas, M.K. Sengupta, D. Lodh, G. Samanta, S. Chakraborty, M.M. Roy, R.N. Dutta, K.C. Saha, S.C. Mukherjee, S. Pati, P.B. Kar, Fate of over 480 million inhabitants living in arsenic and fluoride endemic Indian districts: magnitude, health, socio-economic effects and mitigation approaches, J. Trace Elem. Med. Biol. 38 (2016) 33–45, https://doi.org/10.1016/J.JTEMB.2016.05.001.
[7] A.S. Kraus, W.F. Forbes, Aluminum, fluoride and the prevention of Alzheimer's disease, Can. J. Public Health, 83 (n.d.) 97-100, http://www.ncbi.nlm.nih.gov/pubmed/1617567. accessed February 26, 2019.
[8] A. Bhatnagar, E. Kumar, M. Sillanpää, Fluoride removal from water by adsorption-A review, Chem. Eng. J. 171 (2011) 811–840, https://doi.org/10.1016/j.cej.2011.05.028.
[9] X. Xiong, J. Liu, W. He, T. Xia, P. He, X. Chen, K. Yang, A. Wang, Dose–effect relationship between drinking water fluoride levels and damage to liver and kidney functions in children, Environ. Res. 103 (2007) 112–116, https://doi.org/10.1016/j.envres.2006.05.008.
[10] S. Wickramarathna, S. Balasooriya, S. Diyabalanage, R. Chandrajith, Tracing environmental aetiological factors of chronic kidney diseases in the dry zone of Sri Lanka—a hydrogeochemical and isotope approach, J. Trace Elem. Med. Biol. 44 (2017) 298–306, https://doi.org/10.1016/j.jtemb.2017.08.013.
[11] W.B. Apambire, D.R. Boyle, F.A. Michel, Geochemistry, genesis, and health implications of fluoriferous groundwaters in the upper regions of Ghana, Environ. Geol. 33 (1997) 13–24, https://doi.org/10.1007/s002540050221.
[12] E.J. Reardon, Y. Wang, A limestone reactor for fluoride removal from wastewaters, Environ. Sci. Technol. 34 (2000) 3247–3253, https://doi.org/10.1021/es990542k.
[13] H. Huang, J. Liu, P. Zhang, D. Zhang, F. Gao, Investigation on the simultaneous removal of fluoride, ammonia nitrogen and phosphate from semiconductor wastewater using chemical precipitation, Chem. Eng. J. 307 (2017) 696–706, https://doi.org/10.1016/J.CEJ.2016.08.134.
[14] X. Fan, D.J. Parker, M.D. Smith, Adsorption kinetics of fluoride on low cost materials, Water Res. 37 (2003) 4929–4937, https://doi.org/10.1016/J.WATRES.2003.08.014.
[15] N. Das, P. Pattanaik, R. Das, Defluoridation of drinking water using activated titanium rich bauxite, J. Colloid Interface Sci. 292 (2005) 1–10, https://doi.org/10.1016/j.jcis.2005.06.045.
[16] P.I. Ndiaye, P. Moulin, L. Dominguez, J.C. Millet, F. Charbit, Removal of fluoride from electronic industrial effluent by RO membrane separation, Desalination 173 (2005) 25–32, https://doi.org/10.1016/J.DESAL.2004.07.042.

[17] N.L. Le, S.P. Nunes, Materials and membrane technologies for water and energy sustainability, Sustain. Mater. Technol. 7 (2016) 1–28, https://doi.org/10.1016/J.SUSMAT.2016.02.001.
[18] M. Arora, R.C. Maheshwari, S.K. Jain, A. Gupta, Use of membrane technology for potable water production, Desalination 170 (2004) 105–112, https://doi.org/10.1016/J.DESAL.2004.02.096.
[19] K. Hu, J.M. Dickson, Nanofiltration membrane performance on fluoride removal from water, J. Membr. Sci. 279 (2006) 529–538, https://doi.org/10.1016/J.MEMSCI.2005.12.047.
[20] A. Boubakri, N. Helali, M. Tlili, M. Ben Amor, Fluoride removal from diluted solutions by Donnan dialysis using full factorial design, Kor. J. Chem. Eng. 31 (2014) 461–466, https://doi.org/10.1007/s11814-013-0263-9.
[21] N. Kabay, Ö. Arar, S. Samatya, Ü. Yüksel, M. Yüksel, Separation of fluoride from aqueous solution by electrodialysis: effect of process parameters and other ionic species, J. Hazard Mater. 153 (2008) 107–113, https://doi.org/10.1016/J.JHAZMAT.2007.08.024.
[22] S.M. Maliyekkal, A.K. Sharma, L. Philip, Manganese-oxide-coated alumina: a promising sorbent for defluoridation of water, Water Res. 40 (2006) 3497–3506, https://doi.org/10.1016/J.WATRES.2006.08.007.
[23] A. Teutli-Sequeira, V. Martínez-Miranda, M. Solache-Ríos, I. Linares-Hernández, Aluminum and lanthanum effects in natural materials on the adsorption of fluoride ions, J. Fluor. Chem. 148 (2013) 6–13, https://doi.org/10.1016/J.JFLUCHEM.2013.01.015.
[24] Y. Nie, C. Hu, C. Kong, Enhanced fluoride adsorption using Al (III) modified calcium hydroxyapatite, J. Hazard Mater. (2012) 233–234, https://doi.org/10.1016/J.JHAZMAT.2012.07.020, 194–199.
[25] N. Sakhare, S. Lunge, S. Rayalu, S. Bakardjiva, J. Subrt, S. Devotta, N. Labhsetwar, Defluoridation of water using calcium aluminate material, Chem. Eng. J. 203 (2012) 406–414, https://doi.org/10.1016/J.CEJ.2012.07.065.
[26] C.M. Kanno, R.L. Sanders, S.M. Flynn, G. Lessard, S.C.B. Myneni, Novel apatite-based sorbent for defluoridation: synthesis and sorption characteristics of nano-micro-crystalline hydroxyapatite-coated-limestone, Environ. Sci. Technol. 48 (2014) 5798–5807, https://doi.org/10.1021/es405135r.
[27] M.G. Sujana, S. Anand, Iron and aluminium based mixed hydroxides: a novel sorbent for fluoride removal from aqueous solutions, Appl. Surf. Sci. 256 (2010) 6956–6962, https://doi.org/10.1016/J.APSUSC.2010.05.006.
[28] A.I. Ndé-Tchoupé, R.A. Crane, H.T. Mwakabona, C. Noubactep, K.N. Njau, Technologies for decentralized fluoride removal: testing metallic iron-based filters, Water (Switzerland) 7 (2015) 6750–6774, https://doi.org/10.3390/w7126657.
[29] X. Dou, Y. Zhang, H. Wang, T. Wang, Y. Wang, Performance of granular zirconium–iron oxide in the removal of fluoride from drinking water, Water Res. 45 (2011) 3571–3578, https://doi.org/10.1016/J.WATRES.2011.04.002.
[30] L. Chai, Y. Wang, N. Zhao, W. Yang, X. You, Sulfate-doped Fe3O4/Al2O3 nanoparticles as a novel adsorbent for fluoride removal from drinking water, Water Res. 47 (2013) 4040–4049, https://doi.org/10.1016/J.WATRES.2013.02.057.
[31] L.H. Velazquez-Jimenez, R.H. Hurt, J. Matos, J.R. Rangel-Mendez, Zirconium–carbon hybrid sorbent for removal of fluoride from water: oxalic acid mediated Zr(IV) assembly and adsorption mechanism, Environ. Sci. Technol. 48 (2014) 1166–1174, https://doi.org/10.1021/es403929b.
[32] T. Zhang, Q. Li, H. Xiao, Z. Mei, H. Lu, Y. Zhou, Enhanced fluoride removal from water by non-thermal plasma modified CeO2/Mg–Fe layered double hydroxides, Appl. Clay Sci. 72 (2013) 117–123, https://doi.org/10.1016/J.CLAY.2012.12.003.
[33] T. Zhang, Q. Li, H. Xiao, H. Lu, Y. Zhou, Synthesis of Li–Al layered double hydroxides (LDHs) for efficient fluoride removal, Ind. Eng. Chem. Res. 51 (2012) 11490–11498, https://doi.org/10.1021/ie300863x.
[34] P.-P. Huang, C.-Y. Cao, F. Wei, Y.-B. Sun, W.-G. Song, MgAl layered double hydroxides with chloride and carbonate ions as interlayer anions for removal of arsenic and fluoride ions in water, RSC Adv. 5 (2015) 10412–10417, https://doi.org/10.1039/C4RA15160G.
[35] X. Yu, S. Tong, M. Ge, J. Zuo, Removal of fluoride from drinking water by cellulose@hydroxyapatite nanocomposites, Carbohydr. Polym. 92 (2013) 269–275, https://doi.org/10.1016/J.CARBPOL.2012.09.045.
[36] K. Pandi, N. Viswanathan, Synthesis of alginate bioencapsulated nano-hydroxyapatite composite for selective fluoride sorption, Carbohydr. Polym. 112 (2014) 662–667, https://doi.org/10.1016/J.CARBPOL.2014.06.029.
[37] K. Poovendran, K.S.J. Wilson, M.S. Revathy, A. Ayeshamariam, K. Kaviyarasu, Functionalization effect of HAp with copper (Cu) having excellent dielectric applications, Surface. Interfac. 19 (2020) 100474, https://doi.org/10.1016/j.surfin.2020.100474.
[38] M.S. Fernando, R.M. De Silva, K.M.N. De Silva, Synthesis, characterization, and application of nano hydroxyapatite and nanocomposite of hydroxyapatite with granular activated carbon for the removal of Pb2+ from aqueous solutions, Appl. Surf. Sci. 351 (2015) 95–103, https://doi.org/10.1016/j.apsusc.2015.05.092.
[39] M. Kaviya, P. Ramakrishnan, S.B. Mohamed, R. Ramakrishnan, J. Gimbun, K. M. Veerabadran, M.R. Kuppusamy, K. Kaviyarasu, T.M. Sridhar, et al., Synthesis and characterization of nano-hydroxyapatite/graphene oxide composite materials for medical implant coating applications, Mater. Today Proc. (2020), https://doi.org/10.1016/j.matpr.2020.02.932.
[40] L.E.L. Hammari, A. Laghzizil, P. Barboux, K. Lahlil, A. Saoiabi, Retention of fluoride ions from aqueous solution using porous hydroxyapatite: structure and conduction properties, J. Hazard Mater. 114 (2004) 41–44, https://doi.org/10.1016/j.jhazmat.2004.06.032.
[41] W.P.S.L. Wijesinghe, M.M.M.G.P.G. Mantilaka, T.A.N. Peiris, R.M.G. Rajapakse, K. G.U. Wijayantha, H.M.T.G.A. Pitawala, T.N. Premachandra, H.M.T.U. Herath, R.P. V.J. Rajapakse, Preparation and characterization of mesoporous hydroxyapatite with non-cytotoxicity and heavy metal adsorption capacity, New J. Chem. 42 (2018) 10271–10278, https://doi.org/10.1039/c8nj00673c.
[42] D.O. Costa, S.J. Dixon, A.S. Rizkalla, One- and three-dimensional growth of hydroxyapatite nanowires during sol–gel–hydrothermal synthesis, ACS Appl. Mater. Interfaces 4 (2012) 1490–1499, https://doi.org/10.1021/am201735k.
[43] Y. Zhang, L. Zhou, D. Li, N. Xue, X. Xu, J. Li, Oriented nano-structured hydroxyapatite from the template, Chem. Phys. Lett. 376 (2003) 493–497, https://doi.org/10.1016/S0009-2614(03)01038-8.
[44] X.Y. Zhao, Y.J. Zhu, C. Qi, F. Chen, B.Q. Lu, J. Zhao, J. Wu, Hierarchical hollow hydroxyapatite microspheres: microwave-assisted rapid synthesis by using pyridoxal-5′-phosphate as a phosphorus source and application in drug delivery, Chem. Asian J. 8 (2013) 1313–1320, https://doi.org/10.1002/asia.201300142.
[45] K. Lin, X. Liu, J. Chang, Y. Zhu, Facile synthesis of hydroxyapatite nanoparticles, nanowires and hollow nano-structured microspheres using similar structured hard-precursors, Nanoscale 3 (2011) 3052, https://doi.org/10.1039/c1nr10334b.
[46] H. Lian, L. Zhang, Z. Meng, et al., Biomimetic hydroxyapatite/gelatin composites for bone tissue regeneration: fabrication, characterization, and osteogenic differentiation in vitro, Mater. Des. 156 (2018) 381–388, https://doi.org/10.1016/j.matdes.2018.07.009.
[47] M.M.M.G.P.G. Mantilaka, H.M.T.G.A. Pitawala, R.M.G. Rajapakse, D.G.G. P. Karunaratne, K.G. Upul Wijayantha, et al., Formation of hollow bone-like morphology of calcium carbonate on surfactant/polymer templates, J. Cryst. Growth 392 (2014) 52–59, https://doi.org/10.1016/j.jcrysgro.2014.02.007.
[48] M.M.M.G.P.G. Mantilaka, W.P.S.L. Wijesinghe, H.M.T.G.A. Pitawala, R.M. G. Rajapakse, D.G.G.P. Karunaratne, Surfactant-assisted synthesis of pure calcium carbonate nanoparticles from Sri Lankan dolomite, J. Natl. Sci. Found. Sri Lanka 42 (2014) 221–228, https://doi.org/10.4038/jnsfsr.v42i3.7398.
[49] N.A. Belsey, A.G. Shard, C. Minelli, Surf. Chem. (2016), https://doi.org/10.1002/9781118753460.ch8.
[50] Y.H. Li, S. Wang, X. Zhang, J. Wei, C. Xu, Z. Luan, D. Wu, Adsorption of fluoride from water by aligned carbon nanotubes, Mater. Res. Bull. 38 (2003) 469–476, https://doi.org/10.1016/S0025-5408(02)01063-2.
[51] J.P. Marcolongo, M. Mirenda, Thermodynamics of sodium dodecyl sulfate (SDS) micellization: an undergraduate laboratory experiment, J. Chem. Educ. 88 (2011) 629–633, https://doi.org/10.1021/ed900019u.
[52] E.M. Egorova, S.I. Kaba, The effect of surfactant micellization on the cytotoxicity of silver nanoparticles stabilized with aerosol-OT, Toxicol. Vitro 57 (2019) 244–254, https://doi.org/10.1016/j.tiv.2019.03.006.
[53] R. Palepu, Interaction between Sodium Dodecyl Sulfate (SDS) and Polyvinylpyrrolidone (PVP) Investigated with Forward and Reverse Component Addition Protocols Employing Techniques, 2006, pp. 871–878, https://doi.org/10.1007/s00396-005-1453-8.
[54] V.U. Godakanda, H. Li, L. Alquezar, L. Zhao, L.M. Zhu, R. de Silva, K.M.N. de Silva, G.R. Williams, Tunable drug release from blend poly(vinyl pyrrolidone)-ethyl cellulose nanofibers, Int. J. Pharm. 562 (2019) 172–179, https://doi.org/10.1016/j.ijpharm.2019.03.035.
[55] D.C. Manatunga, R.M. De Silva, K.M.N. De Silva, R. Ratnaweera, Natural polysaccharides leading to super adsorbent hydroxyapatite nanoparticles for the removal of heavy metals and dyes from aqueous solutions, RSC Adv. 6 (2016) 105618–105630, https://doi.org/10.1039/c6ra22662k.
[56] K.S.M. Udayakantha, R.M. De Silva, K.M.N. De Silva, C. Hettiarachchi, Biocompatible nano hydroxyapatite - curcumin bi-coated antibacterial activated carbon for water purification, RSC Adv. 5 (2015) 64696–64703, https://doi.org/10.1039/c5ra11518c.
[57] L.H. Hussin, M.H. Yaakob, N. Osman, N.A. Mazlan, Effect of surfactants on the thermal decomposition of Li 7 La 3 Zr 2 O 12 ceramics 2 (2013) 49–52.
[58] I.W. Siriwardane, R. Udangawa, R.M. De Silva, A.R. Kumarasinghe, R.G. Acres, A. Hettiarachchi, G.A.J. Amaratunga, K.M.N. De Silva, Synthesis and characterization of nano magnesium oxide impregnated granular activated carbon composite for H2S removal applications, Mater. Des. (2017), https://doi.org/10.1016/j.matdes.2017.09.034.
[59] R. Senthil, G. Vijayaragavan, A. Ayeshamariam, K. Kaviyarasu, Nonlinear optical properties of single crystal of L-OOMHCL incorporation with Glycine Oxalic Acid (Goa) with high chemical stability for optoelectronic applications, Surface. Interfac. 18 (2020) 100417, https://doi.org/10.1016/j.surfin.2019.100417.
[60] K. Kaviyarasu, A. Mariappan, K. Neyvasagam, A. Ayeshamariam, P. Pandi, R. R. Palanichamy, C. Gopinathan, G.T. Mola, M. Maaza, Photocatalytic performance and antimicrobial activities of HAp-TiO2 nanocomposite thin films by sol-gel method, Surface. Interfac. 6 (2017) 247–255, https://doi.org/10.1016/j.surfin.2016.10.002.
[61] X. Fan, D.J. Parker, M.D. Smith, Adsorption kinetics of fluoride on low cost materials, Water Res. 37 (2003) 4929–4937, https://doi.org/10.1016/j.watres.2003.08.014.
[62] N. Chen, Z. Zhang, C. Feng, M. Li, D. Zhu, N. Sugiura, Studies on fluoride adsorption of iron-impregnated granular ceramics from aqueous solution, Mater. Chem. Phys. 125 (2011) 293–298, https://doi.org/10.1016/j.matchemphys.2010.09.037.
[63] N.M.I. Alhaji, D. Nathiya, K. Kaviyarasu, M. Meshram, A. Ayeshamariam, A comparative study of structural and photocatalytic mechanism of AgGaO2 nanocomposites for equilibrium and kinetics evaluation of adsorption parameters, Surface. Interfac. 17 (2019) 100375, https://doi.org/10.1016/j.surfin.2019.100375.
[64] Y.S. Ho, G. McKay, Pseudo-second order model for sorption processes, Process Biochem. 34 (1999) 451–465, https://doi.org/10.1016/S0032-9592(98)00112-5.

[65] S. Gao, R. Sun, Z. Wei, H. Zhao, H. Li, F. Hu, et al., Size-dependent defluoridation properties of synthetic hydroxyapatite, J. Fluor. Chem. 130 (2009) 550–556, https://doi.org/10.1016/j.jfluchem.2009.03.007.
[66] Ö. Neşe, K.T. Ennil, A kinetic study of nitrite adsorption onto sepiolite and powdered activated carbon, Desalination 223 (2008) 174–179, https://doi.org/10.1016/j.desal.2007.01.209.
[67] K. Li, X. Wang, Adsorptive removal of Pb(II) by activated carbon prepared from Spartina alterniflora: equilibrium, kinetics and thermodynamics, Bioresour. Technol. 100 (2009) 2810–2815, https://doi.org/10.1016/j.biortech.2008.12.032.
[68] G. Atun, T. Sismanoglu, Adsorption of 4,4' - iso propylidene diphenol and diphenylolpropane 4,4' dioxyaceticacid from aqueous solution on kaolinite, J. Environ. Sci. Heal. . Part A Environ. Sci. Eng. Toxicol. 31 (1996) 2055–2069, https://doi.org/10.1080/10934529609376474.
[69] B.H. Hameed, M.I. El-Khaiary, Malachite green adsorption by rattan sawdust: isotherm, kinetic and mechanism modeling, J. Hazard Mater. 159 (2008) 574–579, https://doi.org/10.1016/j.jhazmat.2008.02.054.
[70] I. Tsibranska, E. Hristova, Comparison of different kinetic models for adsorption of heavy metals onto activated carbon from apricot stones, Bulg. Chem. Commun. 43 (2011) 370–377, https://doi.org/10.1364/AO.27.003679.
[71] X. Yang, B. Al-Duri, Kinetic modeling of liquid-phase adsorption of reactive dyes on activated carbon, J. Colloid Interface Sci. 287 (2005) 25–34, https://doi.org/10.1016/j.jcis.2005.01.093.
[72] V. Sternitzke, R. Kaegi, J.N. Audinot, E. Lewin, J.G. Hering, C.A. Johnson, Uptake of fluoride from aqueous solution on nano-sized hydroxyapatite: examination of a fluoridated surface layer, Environ. Sci. Technol. 46 (2012) 802–809, https://doi.org/10.1021/es202750t.
[73] T. Aoba, The effect of fluoride on apatite structure and growth, Crit. Rev. Oral Biol. Med. 8 (1997) 136–153, https://doi.org/10.1177/10454411970080020301.
[74] S. Emin, E. Pavlica, H. Okuyucu, M. Valant, G. Bratina, Charge carrier transport in polycrystalline CH3NH3PbI3 perovskite thin films in a lateral direction characterized by time-of-flight photoconductivity, Mater. Chem. Phys. 220 (2018) 182–189, https://doi.org/10.1016/j.matchemphys.2018.08.012.
[75] M.S. Fernando, A.K.D.V.K. Wimalasiri, S.P. Ratnayake, J.M.A.R.B. Jayasinghe, G. R. William, D.P. Dissanayake, K.M.N. De Silva, R.M. De Silva, Improved nanocomposite of montmorillonite and hydroxyapatite for defluoridation of water, RSC Adv. 9 (2019), https://doi.org/10.1039/c9ra03981c.
[76] J. Wang, W. Xu, L. Chen, Y. Jia, L. Wang, X. Huang, J. Liu, Excellent fluoride removal performance by CeO 2 – ZrO 2 nanocages in water environment 231 (2013) 198–205, https://doi.org/10.1016/j.cej.2013.07.022.
[77] A. Nagaraj, M.A. Munusamy, M. Ahmed, S. Suresh Kumar, M. Rajan, Hydrothermal synthesis of a mineral-substituted hydroxyapatite nanocomposite material for fluoride removal from drinking water, New J. Chem. 42 (2018) 12711–12721, https://doi.org/10.1039/c8nj02401d.